Hydrogel Electrolyte with Electron/Ion Dual Regulation Mechanism for Highly Reversible Flexible Zinc Batteries

Fusheng Luo,‡[a] Song Yang,‡[a] Qing Wu,[a] Yue Li,[a] Jinlong Zhang,[a] Yanhui Zhang,[a] Jun Huang,[a]* Haibo Xie,[a]* and Yiwang Chen[b,c]*

[a]Department of Polymeric Materials & Engineering, College of Materials & Metallurgy, Guizhou University, Huaxi District, Guiyang 550025, P. R. China.
E-mail: huangj@gzu.edu.cn, hbxie@gzu.edu.cn.
[b]Institute of Polymers and Energy Chemistry (IPEC)/Film Energy Chemistry for Jiangxi Provincial Key Laboratory (FEC), Nanchang University, 999 Xuefu Avenue, Nanchang, 330031, China.
[c]Key Laboratory of Fluorine and Silicon for Energy Materials and Chemistry of Ministry of Education, Jiangxi Normal University, 99 Ziyang Avenue, Nanchang, 330022, China.
E-mail: ywchen@ncu.edu.cn.

‡ These authors contributed equally to this work.

Experimental Section

Chemicals and materials. Acrylamide (AM) (purity > 99% AR grade, macklin), carboxylated multi-walled carbon nanotubes (MWCNTs) (95%, XianFengNaMi), ammonium persulfate (AR grade, aladdin), $ZnSO_4 \cdot 7H_2O$ (purity > 99%, aladdin), glass fiber membrane (GF-A, Olegee technology, Olegeeino), N,N-methylenebisacrylamide (CP grade, aladdin), Zn foil (100 μm), ammonium acetate (AR grade, aladdin), manganese acetate (AR grade, aladdin).

Preparation of PAM + varying concentrations MWCNTs hydrogel electrolytes. MWCNTs (0, 1, 2, 4, and 6 mg) were combined with 10 mL deionized water ultrasound under 1500 W power for one hour to create MWCNTs dispersed solutions with different concentrations of 0, 0.1, 0.2, 0.4 and 0.6 mg mL^{-1}, respectively. Subsequently, 3.3 g AM, 5.75 g $ZnSO_4$ $7H_2O$, 13.3 mg of ammonium persulfate and 2 mg of N,N-methylenebisacrylamide was added successively. Afterward, the solutions were completely stirred and the mixed solutions were transfer to a 60 ℃ oven for 2 h to complete the polymerization process.

Preparation of MnO_2 cathode. The MnO_2 cathode is fabricated on carbon paper using an electrodeposition process in three-electrode system. A solution was prepared by combining manganese acetate (0.1 M) and ammonium acetate (0.1 M). Subsequently, saturated silver chloride served as the reference electrode, platinum sheet electrodes as counter electrodes and carbon cloth as the working electrode. Finally, electrodeposited at a current density of 5 mA cm^{-2} for 15 minutes. The deposited carbon cloth was placed in a 60 ℃ oven to dry for 12 h to obtain the MnO_2 cathode. The mass loading of MnO_2 is about 1.1 mg cm^{-2}.

Materials Characterization. The morphology of the materials was examined using a scanning electron microscope (FE-SEM, JSM-7500F). For the inner molecular structure of the gel electrolyte, a Fourier transform infrared spectrometer (FTIR, Nicolet iS50) was implemented.

An optical microscope (UB200i) and an atomic force microscope (AFM, Bruker Dimension ICON) were employed to characterize the Zn anode. X-ray diffraction patterns were obtained by XRD (BrukerAXS D8 with Cu Kα radiation at 45 kV). The X-ray photoelectron spectroscopy (XPS) of Zn anodes were implemented by an ESCALab MKII X-ray photoelectron spectrometer. The tensile and compressive tests were conducted at room temperature using a universal testing equipment (AGX-V2).

Electrochemical Measurements. The CR2032 cells were constructed by sandwiching a variety of electrolytes between two electrodes, whereas the cells containing 2 M $ZnSO_4$ electrolyte were separated using glass fiber. The ion conductivity, cyclic voltammetry (CV), electrochemical impedance spectroscopy (EIS), electric double layer capacitance (EDLC), Zn^{2+} ions transference number, Tafel plot, and LSV experiments were conducted using the electrochemical workstation (CHI 760E). In particular, CV curves were obtained at a scan rate of 0.1 mV s^{-1}. EIS and ion conductivity measurements were conducted within the frequency range of 100 kHz to 0.1 Hz. The Tafel plot and LSV curve were evaluated at a scan rate of 5 mV s^{-1} using a two-electrode configuration.

COMSOL computational details. In order to simulate the dynamic Zn deposition on electrodes in different electrolytes, a Finite Element Analysis model was performed using COMSOL 6.1 software with the "phase field" and "partial differential equation" module. The size of the entire two-dimensional model for electric field distribution analysis was set to 6 × 4 μm. A transient simulation of the process was carried out in an area filled with electrolyte. The initial concentration was 1000 mol/m^3, the electrode conductivity was 10^7 S/m, the interface mobility of the unoptimized model was 10^{-6} m·s/kg, and the interface mobility of the optimized structure was 4×10^{-6} m·s/kg. The distribution of phase volume fraction, ion concentration and

electric field are obtained by simulation. Grid division: The complete grid contains 16714 domain units and 334 boundary units.

Calculation detail. In order to test the ionic conductivity, the hydrogel electrolytes were sandwiched between two plates of symmetric stainless steel for the EIS measurement. After that, the equation of ionic conductivity (σ) was calculated by

$$\sigma = \frac{L}{SR} \quad (1)$$

where L and S represent the thickness and the test area of hydrogel electrolytes, R is the bulk resistance derived from the high-frequency intercept of the semi-circle in EIS plot.

The capacitance (C) is determined by the linear relationship between capacitive current (i_c) and scan rate (v), which can be obtained from the slope of the i_c versus v graphs. Therefore, the EDL capacitance was calculated through the following equation:

$$C = \frac{i_c}{v} \quad (2)$$

Where i_c refers to the capacitive currents in CV scans. Here, we choose $i_c=(i_0^{v+}-i_0^{v-})/2$, meaning half value of current difference during forward scan and negative scan at 0 V. v refers to the scan rates of CV tests.[1] Here, we selected 4, 6, 8, 10, 12 mV s^{-1} as the scan rates respectively. Corresponding CV was measured by scanning between -15 and 15 mV with Zn//Zn symmetric cells. Subsequently, the desolvation energy (E_a) was obtained according to the Arrhenius equation:

$$\frac{1}{R_{ct}} = A\exp\left(-\frac{E_a}{RT}\right) \quad (3)$$

where R_{ct} is the charge transfer resistance, A is the pre-exponential constant, T is the absolute temperature, and R is the standard gas constant. It should be noted that the hydrogels were incubated under a series of temperatures of 40, 50, 60, 70, and 80 °C before measurements. In addition, the I-t measurement of Zn//Zn symmetrical battery was carried out by setting a

constant voltage of 10 mV for 10000 s, followed by another alternating-current (AC) impedance measurement. The Zn^{2+} ions transference number (t) was obtained by the following equation:

$$t = \frac{I_s(\Delta v - I_0 R_0)}{I_0(\Delta v - I_s R_s)} \quad (4)$$

where Δv is the constant voltage, R_0 and R_s represent the initial and steady-state charge transfer resistances, and I_0 and I_s represent the initial and steady-state current, respectively. We also examine a parameter known as compounded CE to more accurately represent the behavior of the Zn//Cu asymmetric cell over multiple cycles,[2-4] as indicated by the following equation:

$$Cumulative\ CE = 100 \times \prod_{1}^{n} \frac{Q_{strip,n}}{Q_{plate,n}} \quad (5)$$

Where n is the number of cycles and $Q_{strip,n}$ and $Q_{plate,n}$ are the stripped and plated charges at each nth cycle, respectively. In order to accurately evaluate the kinetics of Zn electrodeposition process, the exchange current density was calculated by the equation:

$$i \approx i_0 \frac{F}{RT} \cdot \frac{\eta}{2} \quad (6)$$

where i and i_0 are running current density and the exchange current density, respectively, F is the Faradic constant, R is the gas constant, T is the Kelvin temperature, and η is total overpotential.

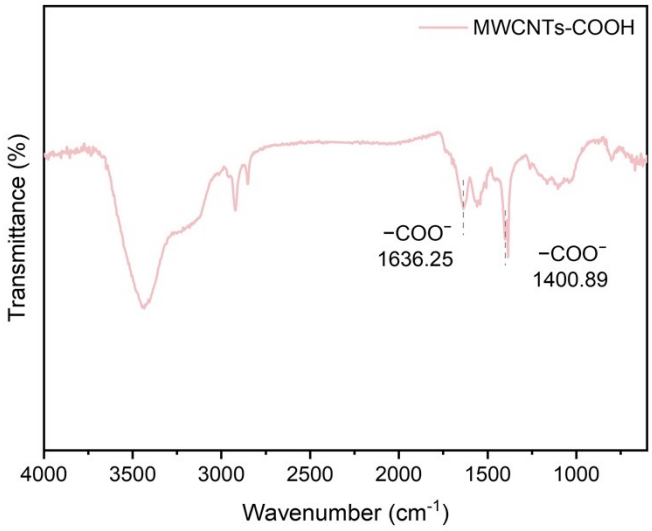

Fig. S1 FTIR spectra of MWCNTs.

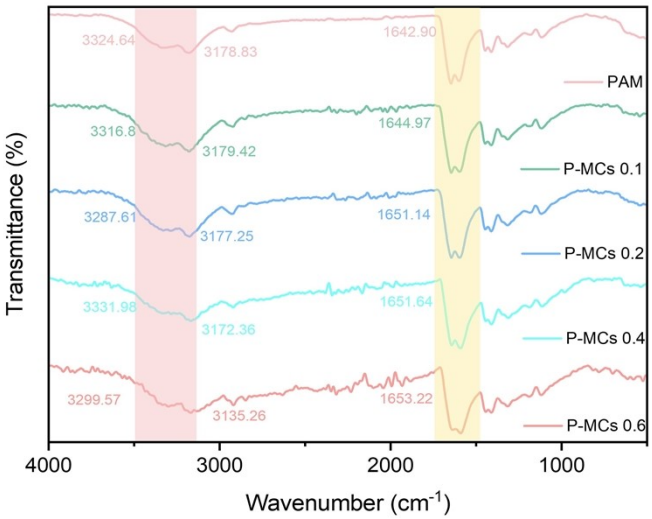

Fig. S2 FTIR spectra of PAM hydrogels with different MWCNTs contents.

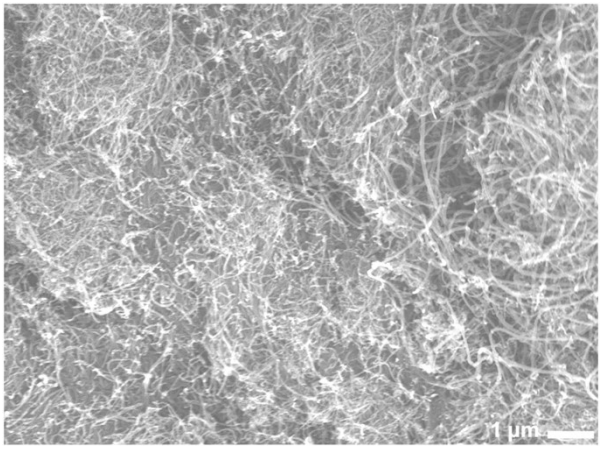

Fig. S3 SEM image of MWCNTs.

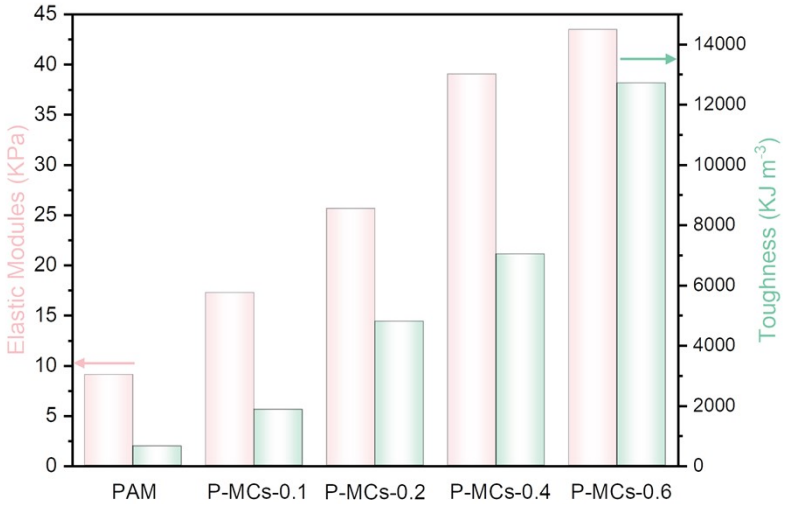

Fig. S4 The elastic modulus and toughness of PAM hydrogels with different MWCNTs contents.

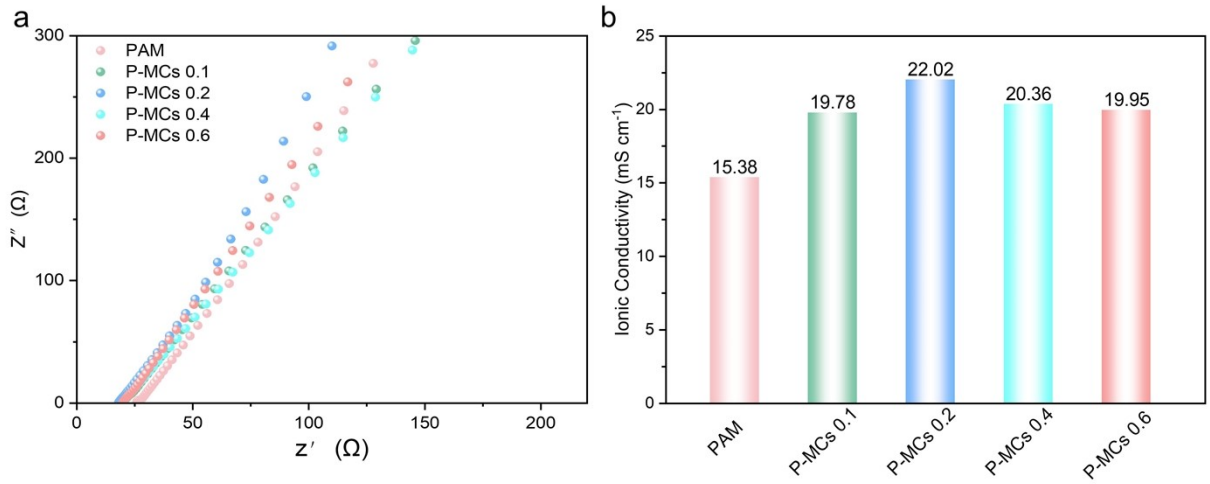

Fig. S5 (a) EIS curves and (b) ionic conductivities of PAM hydrogel electrolytes with different MWCNTs contents.

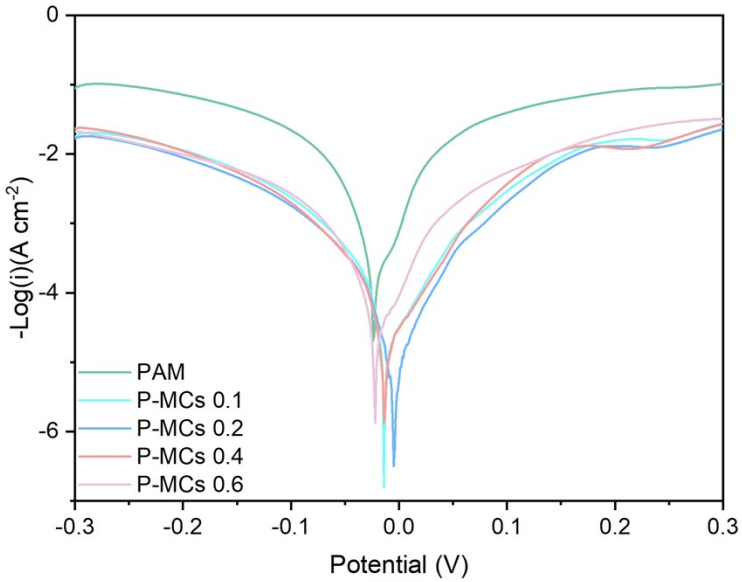

Fig. S6 Tafel curves of PAM hydrogel electrolytes with different MWCNTs contents.

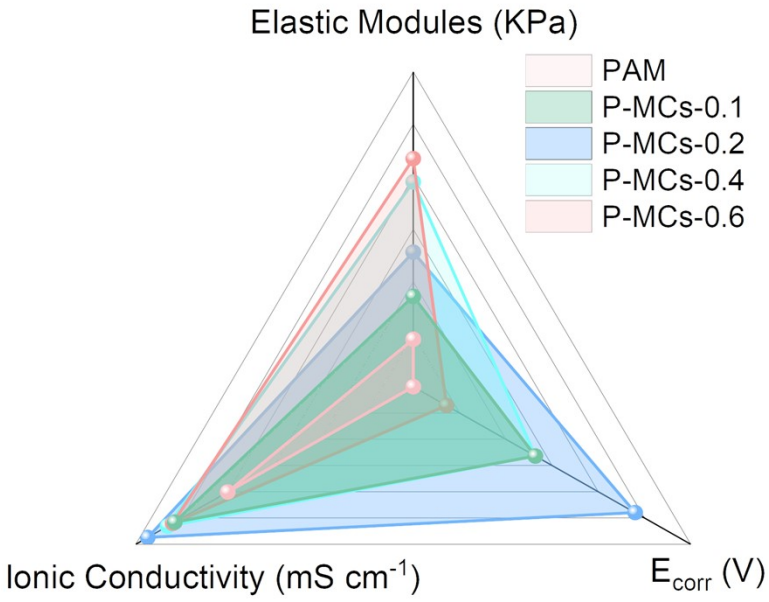

Fig. S7 The radar chart of PAM hydrogels with different MWCNTs contents in terms of elastic, corrosion potential and ionic conductivity.

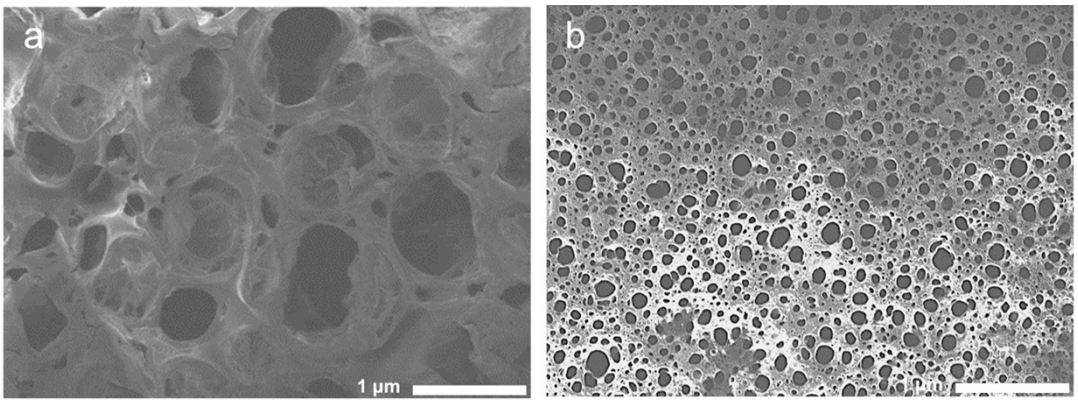

Fig. S8 SEM images of (a) PAM and (b) P-MCs hydrogels after the freeze-drying process.

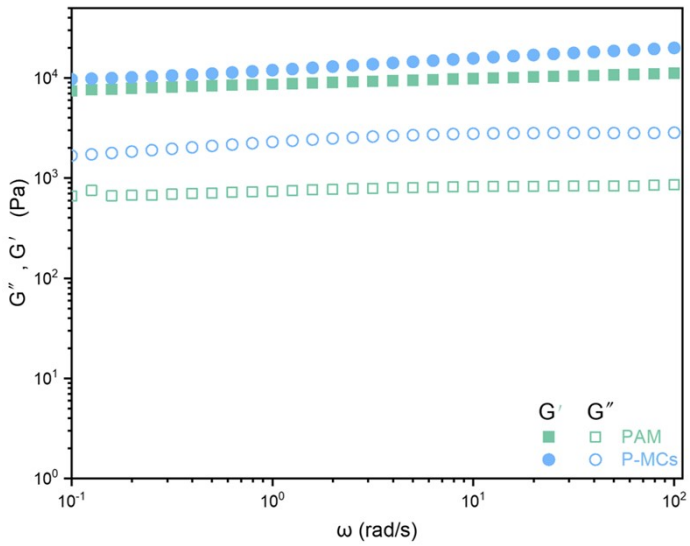

Fig. S9 Rheological behavior of different hydrogels.

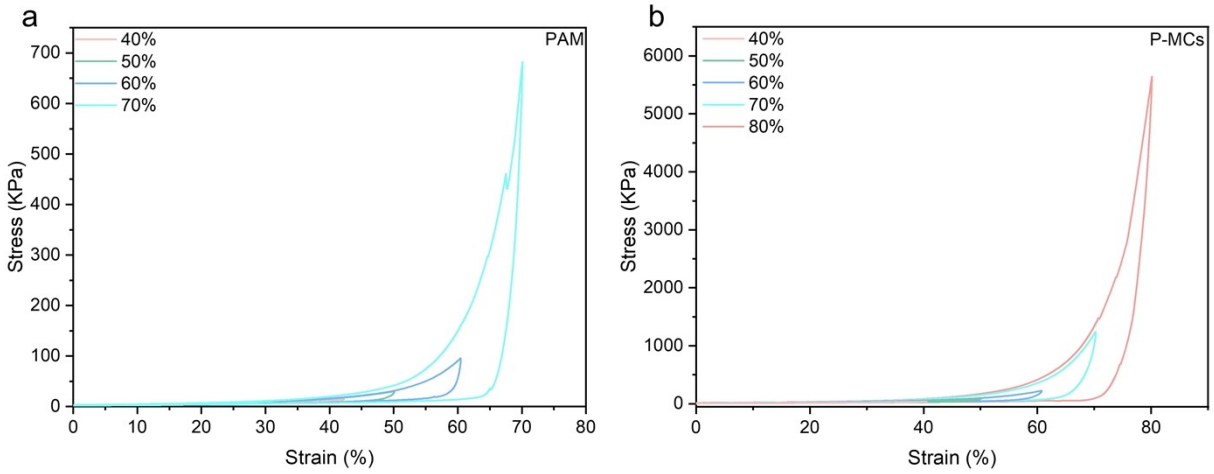

Fig. S10 Compressive stress-strain curves of (a) PAM and (b) P-MCs hydrogels under various strains.

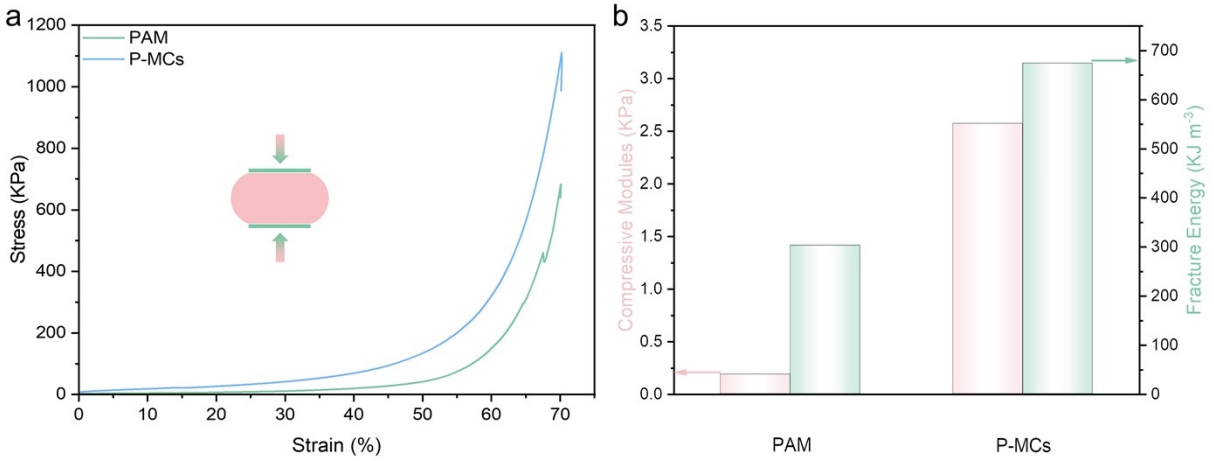

Fig. S11 (a) Compressive stress-strain curves and (b) the corresponding fracture energy and compressive modulus of PAM and P-MCs hydrogels.

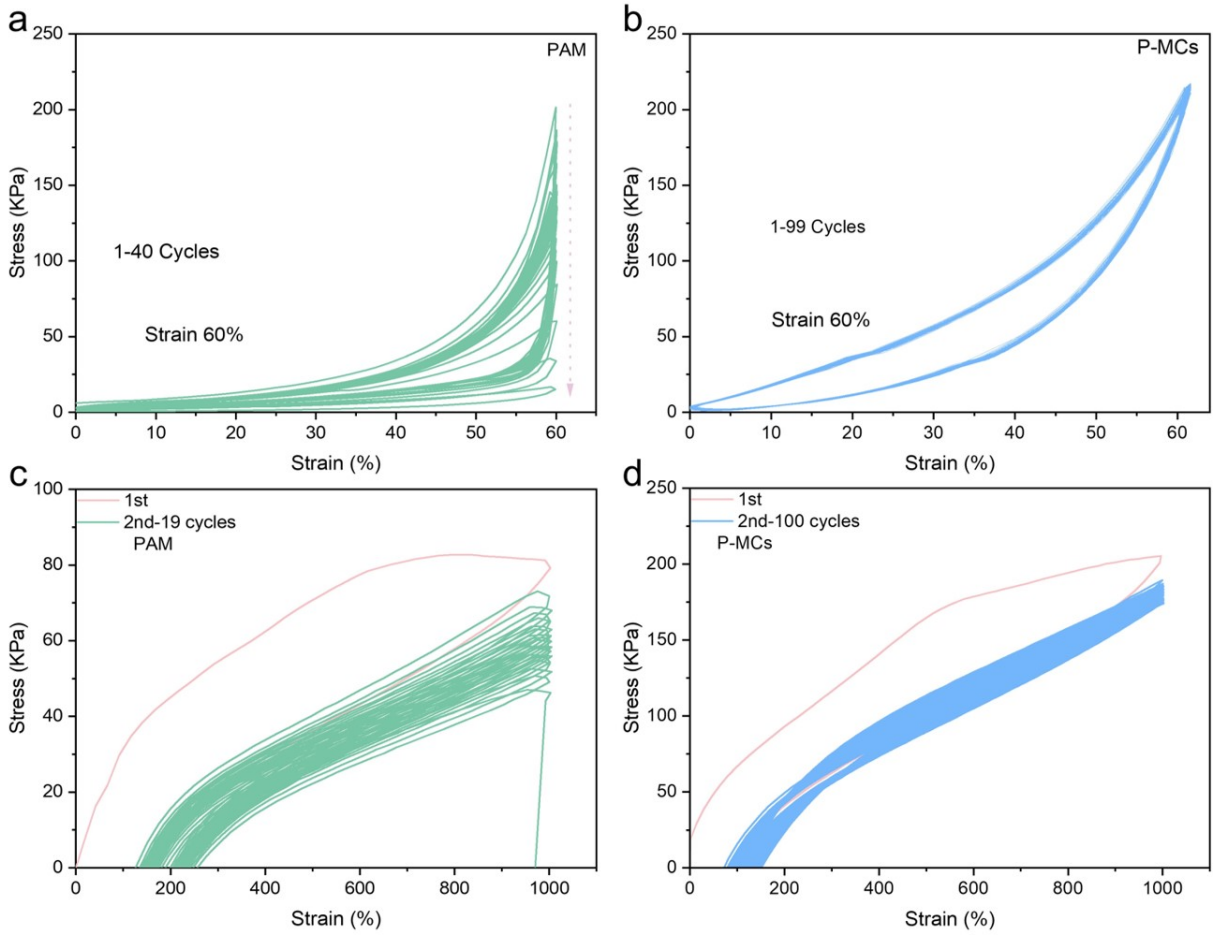

Fig. S12 Cyclic compressive stress-strain curves of the (a) PAM and (b) P-MCs hydrogels under a strain of 60%. Cyclic tensile stress-strain curves of (c) PAM and (d) P-MCs hydrogels under a strain of 1000%.

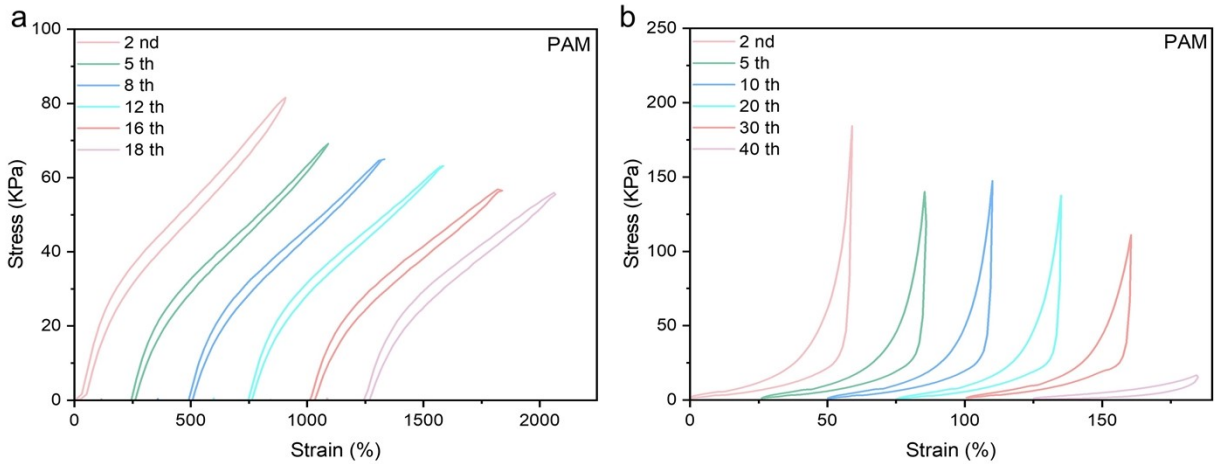

Fig. S13 (a) Tensile stress-strain curves of PAM hydrogel under different cycles at 1000% strain. (b) Compressive stress-strain curves of PAM hydrogel under different cycles at 60% strain.

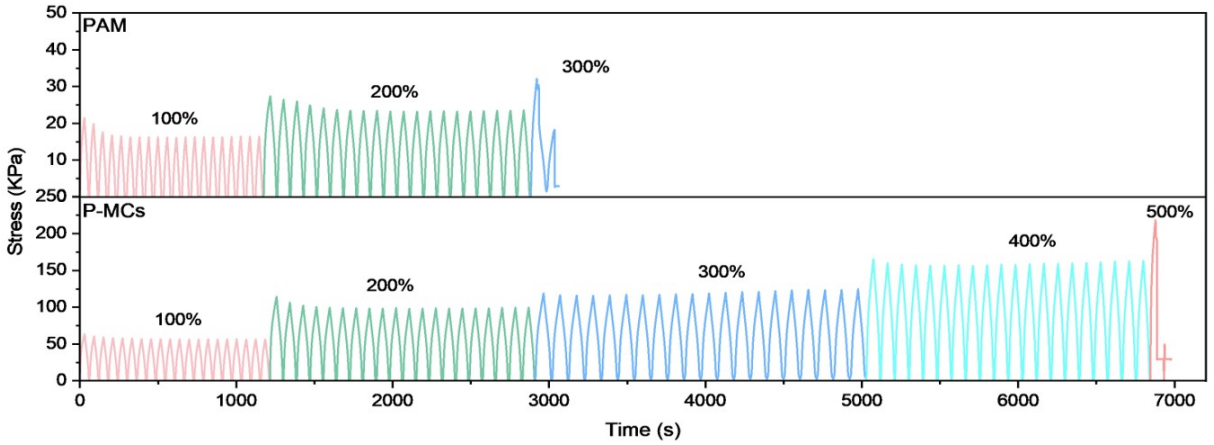

Fig. S14 Change in stress for precut PAM and P-MCs hydrogels under different strains.

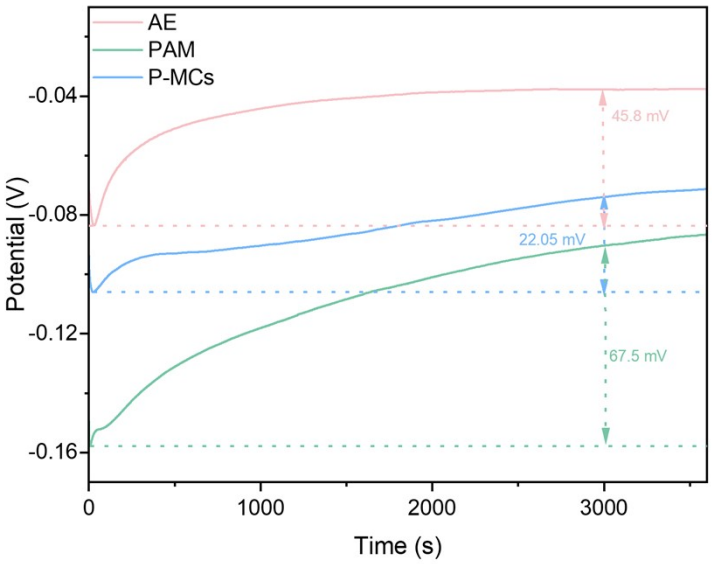

Fig. S15 The NOP of the Zn//Zn symmetric cells in different electrolytes.

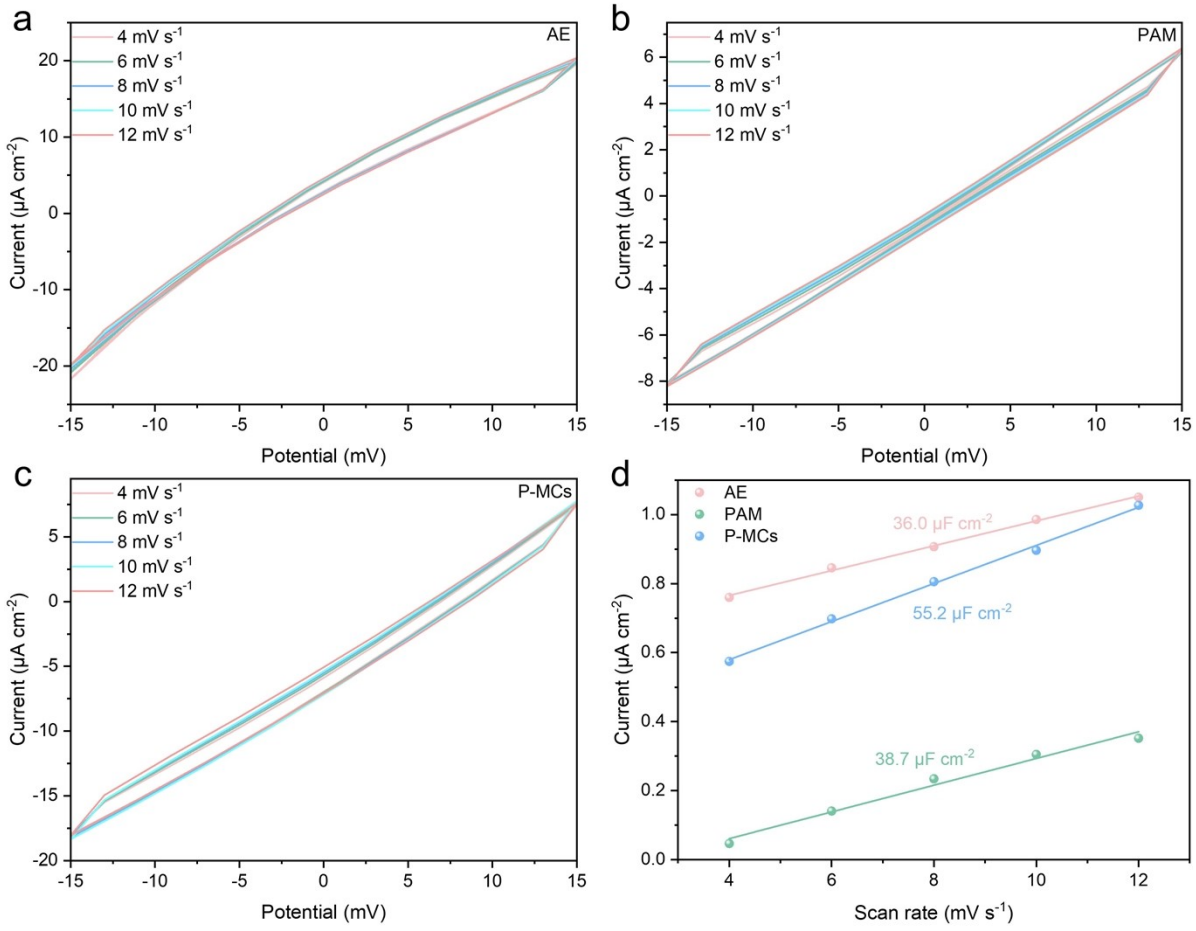

Fig. S16 CV curves for Zn//Zn symmetric cells in the voltage range of -15 mV to 15 mV under various scanning rates in (a) AE, (b) PAM hydrogel electrolyte and (c) P-MCs hydrogel electrolyte. (d) EDLC of different electrolytes.

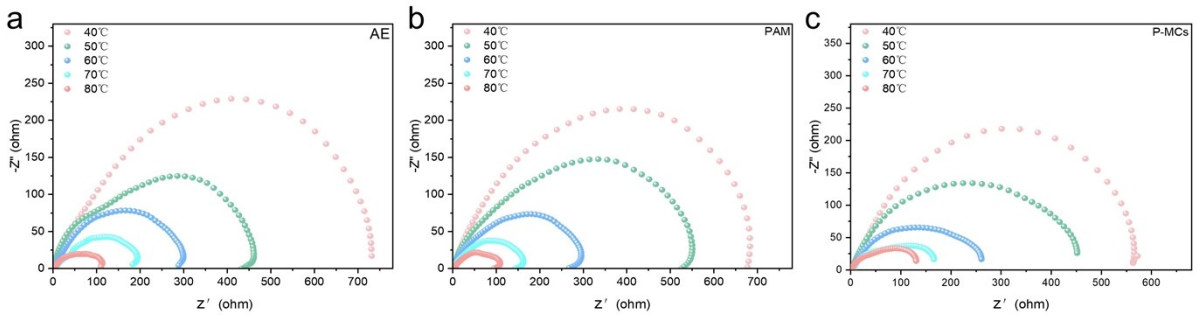

Fig. S17 EIS curves of (a) AE, (b) PAM hydrogel electrolyte and (c) P-MCs hydrogel electrolyte at different temperatures.

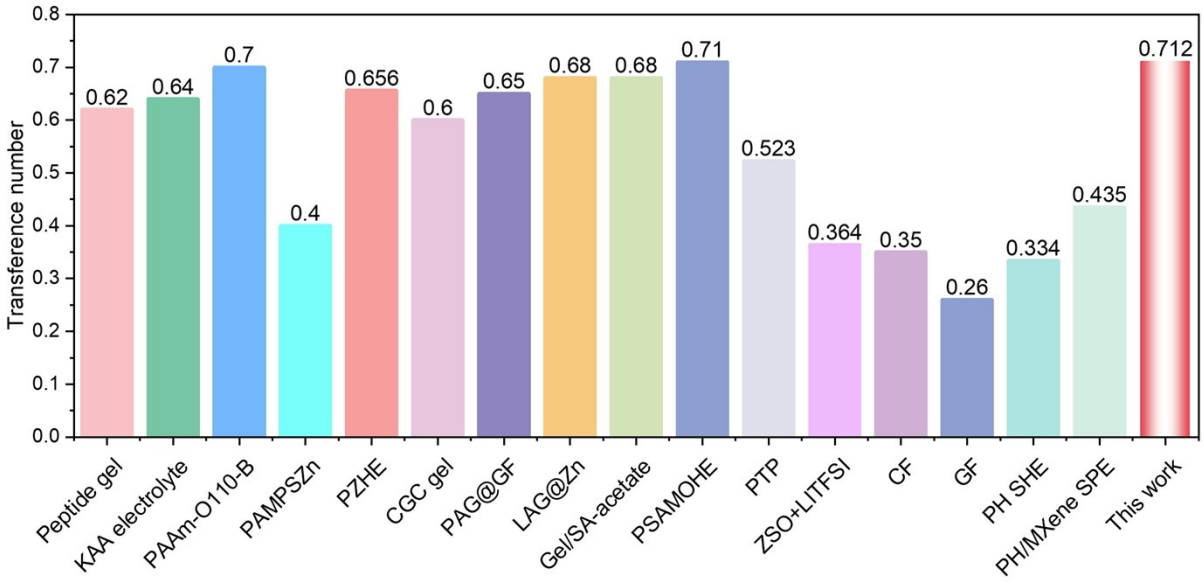

Fig. S18 Comparison of the Zn^{2+} transference number of P-MCs hydrogel electrolyte with other reports.[5-18]

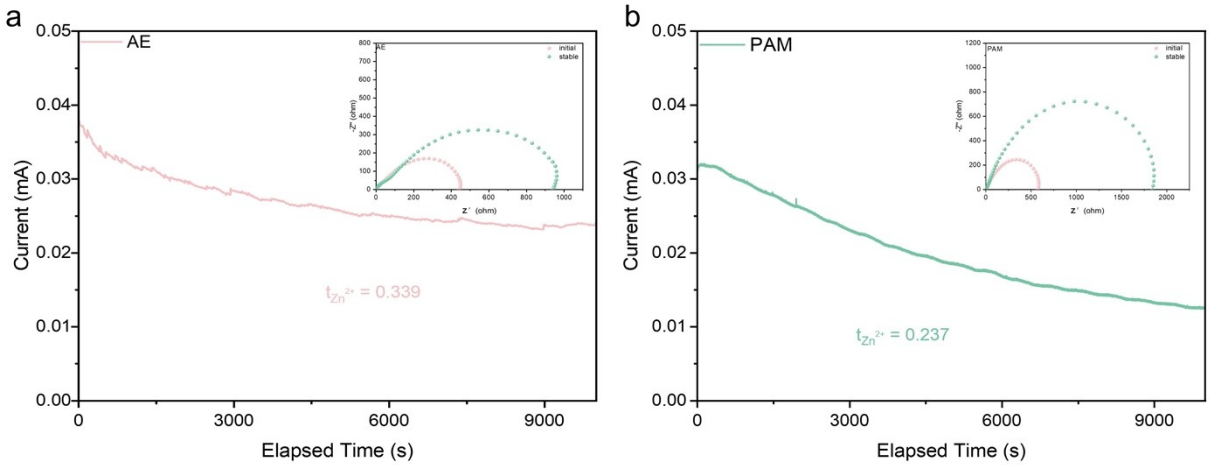

Fig. S19 CA measurement results and EIS curves before and after CA measurements of (a) AE and (b) PAM hydrogel electrolyte.

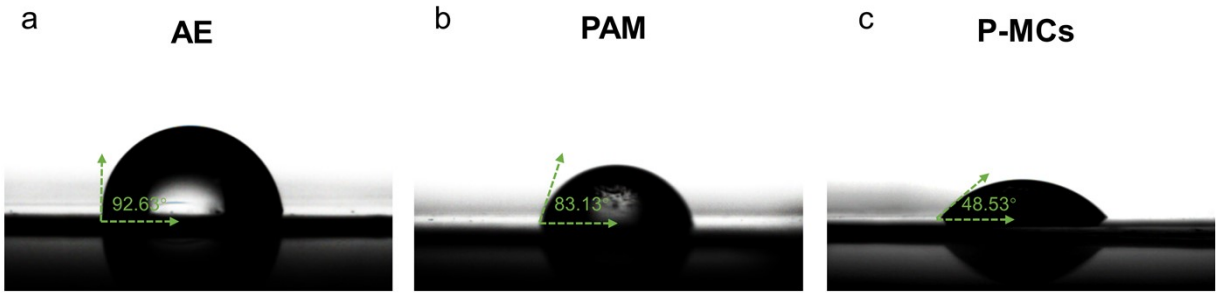

Fig. S20 Contact angles of (a) AE, (b) PAM and (c) P-MCs prepolymers dropped on to the surface of Zn foil.

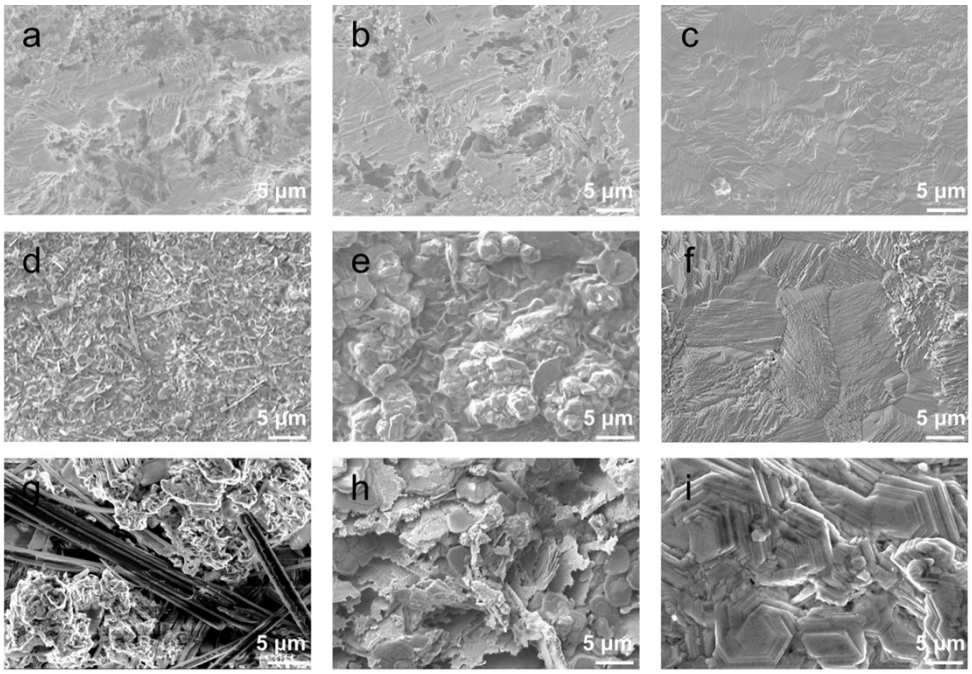

Fig. S21 SEM images of Zn anodes using (a, d, g) AE, (b, c, h) PAM hydrogel electrolyte and (c, f, i) P-MCs hydrogel electrolyte after (a-c) 20, (d-f) 40 and (g-i) 60 cycles at 5 mA cm^{-2} and 5 mAh cm^{-2}, respectively.

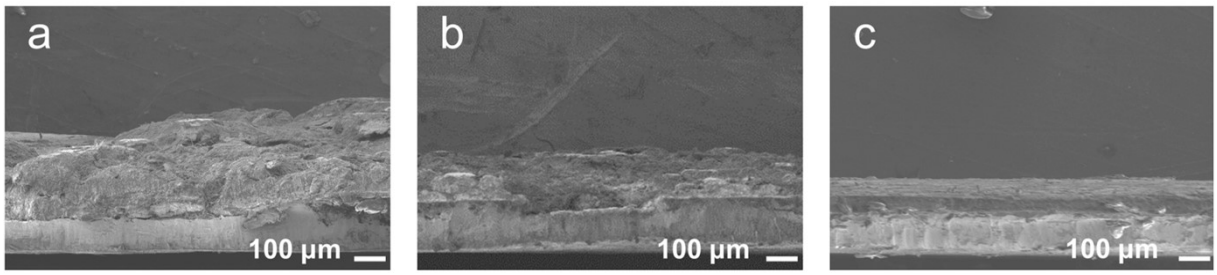

Fig. S22 Cross-sectional SEM images of Zn anodes after 60 cycles in different electrolytes: (a) AE, (b) PAM hydrogel electrolyte and (c) P-MCs hydrogel electrolyte at 5 mA cm^{-2} and 5 mAh cm^{-2}.

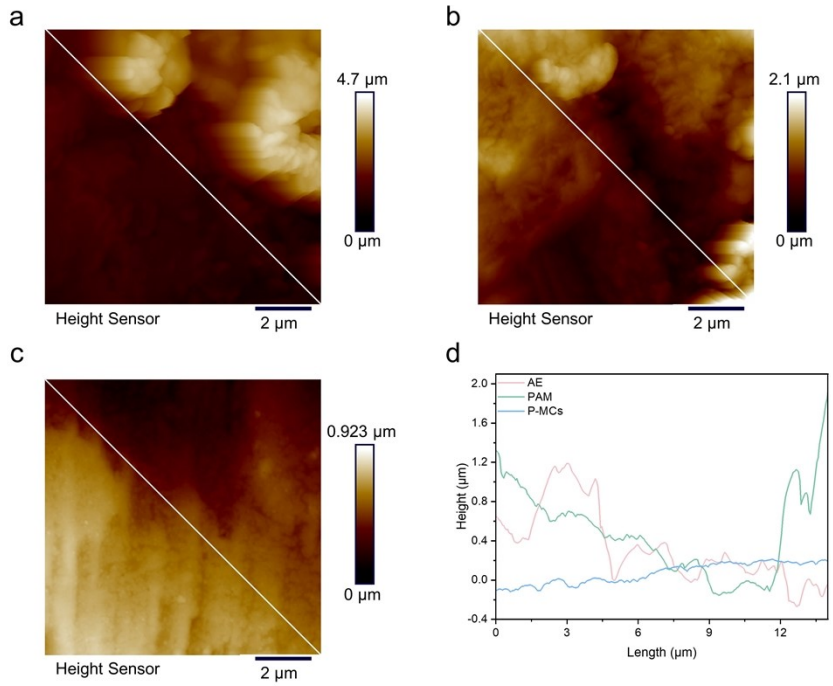

Fig. S23 2D AFM images of Zn anodes with (a) AE, (b) PAM hydrogel electrolyte and (c) P-MCs hydrogel electrolyte after 60 cycles at 5 mA cm^{-2} and 5 mAh cm^{-2}. (d) The corresponding thickness of the area where the line is drawn.

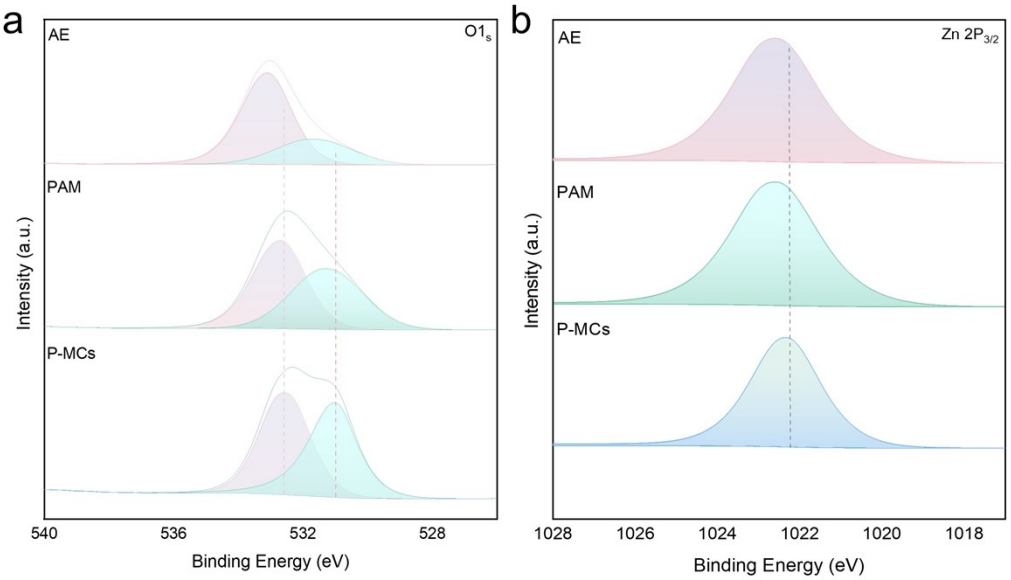

Fig. S24 XPS spectra of (a) O 1s and (b) Zn $2p_{3/2}$ for different electrolytes.

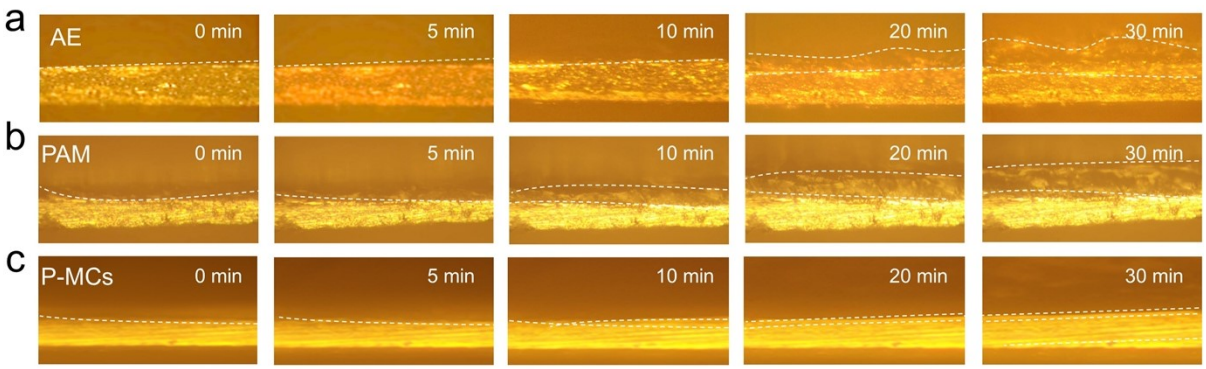

Fig. S25 *In-situ* optical microscope measurements of Zn electrodeposition at 5 mA cm^{-2} for 30 min in (a) AE, (b) PAM hydrogel electrolyte and (c) P-MCs hydrogel electrolyte.

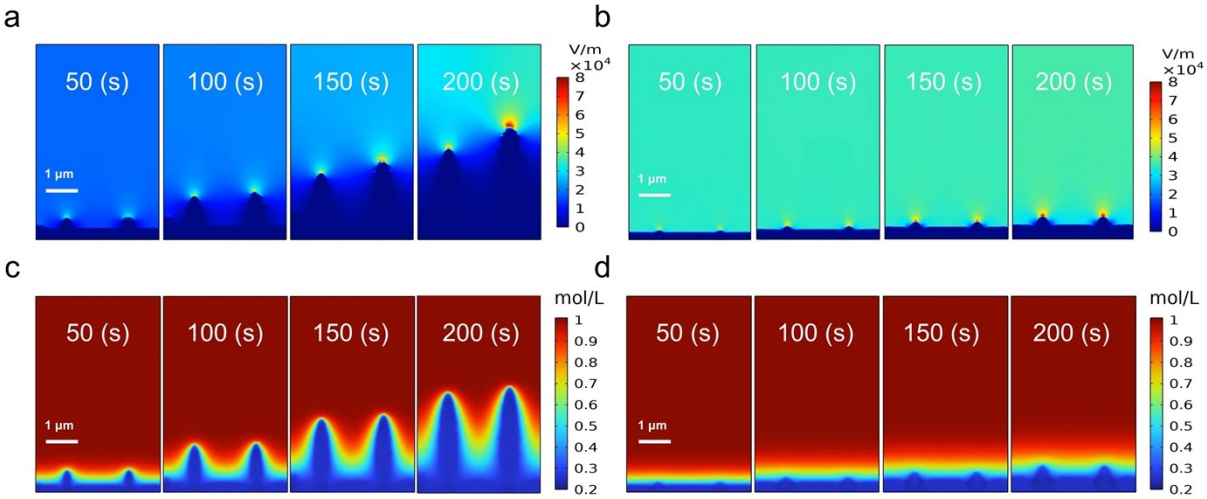

Fig. S26 Electric field of (a) PAM and (b) P-MCs hydrogel electrolytes and the corresponding Zn^{2+} ions concentration of (c) PAM and (d) P-MCs hydrogel electrolytes after Zn electrodeposition for 50, 100, 150 and 200 s, respectively.

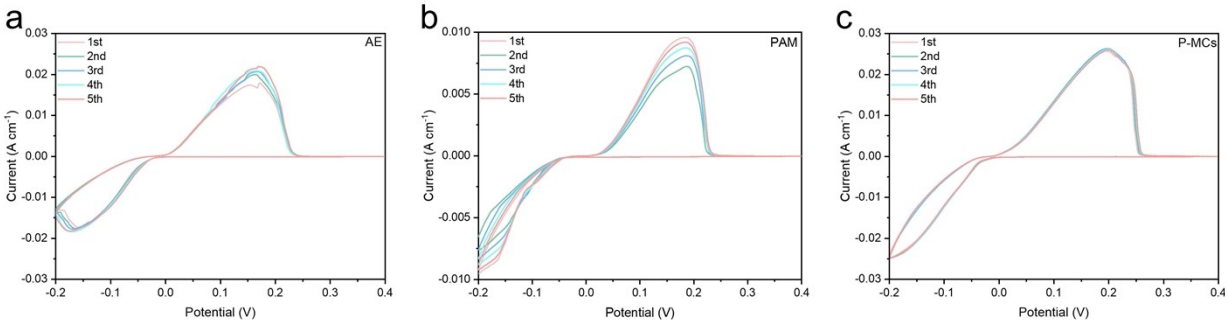

Fig. S27 (a-c) CV curves for Zn//Cu asymmetric cells under different cycles with different electrolytes.

Fig. S28 (a-c) *In-situ* EIS curves of Zn//Cu asymmetric cells with different electrolytes.

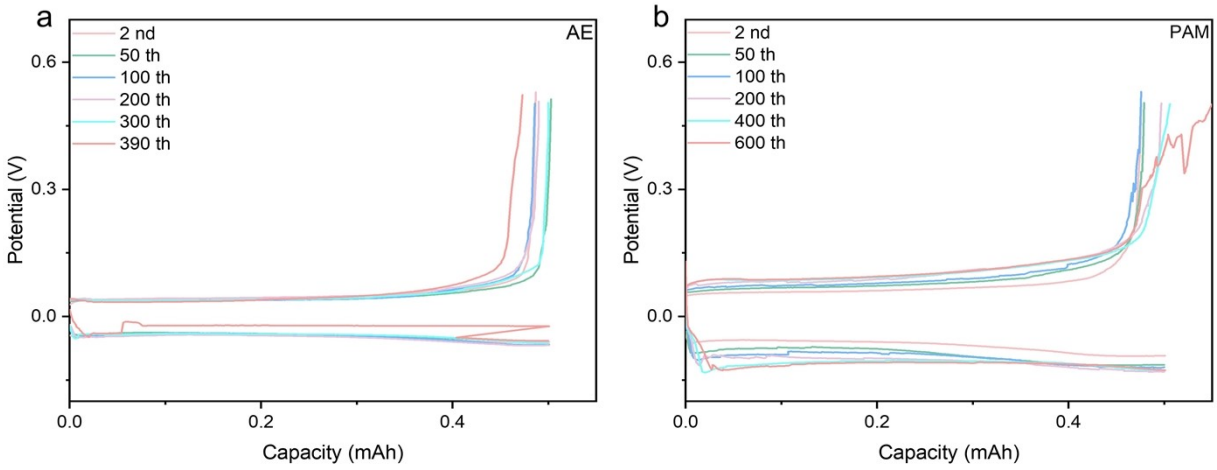

Fig. S29 The corresponding potential/capacity curves for Zn//Cu asymmetric cells with (a) AE and (b) PAM hydrogel electrolyte at different cycles.

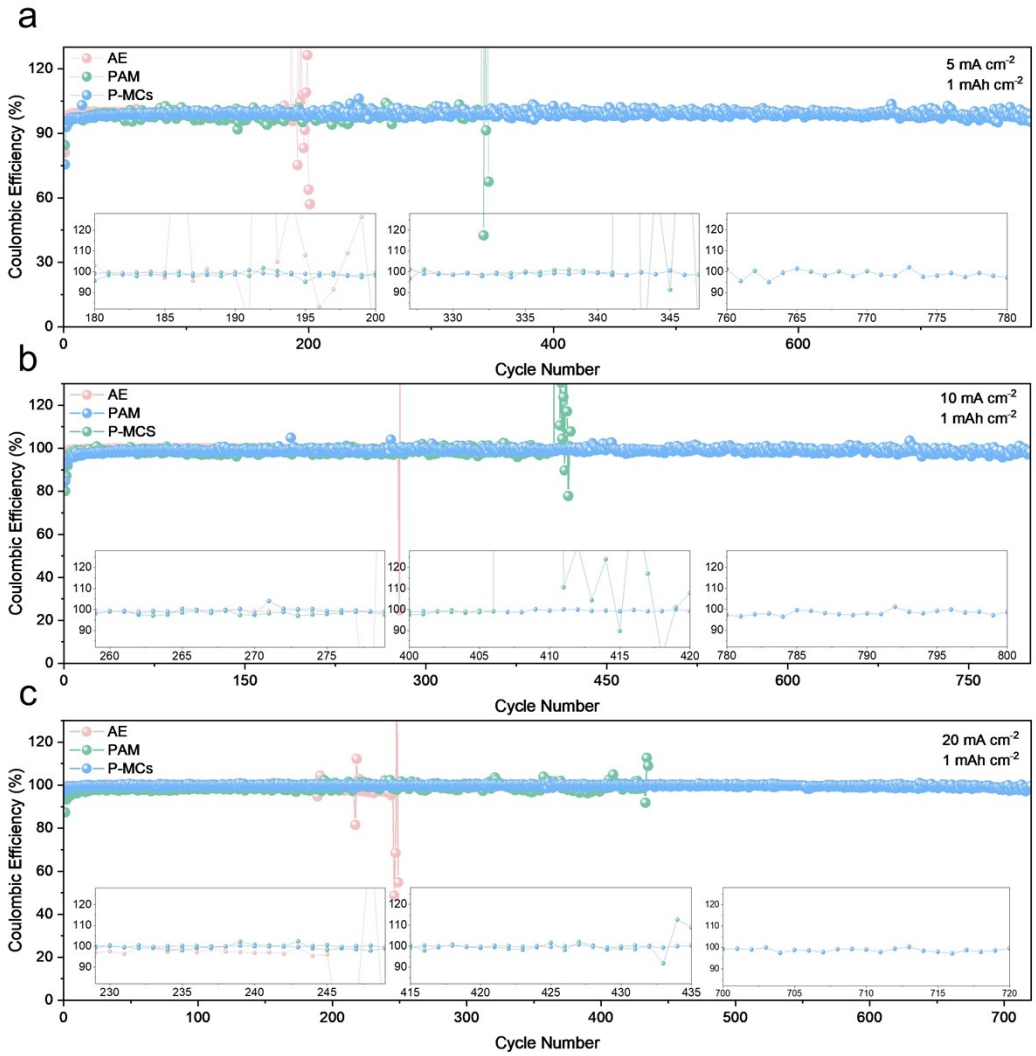

Fig. S30 (a-c) The CEs for Zn//Cu asymmetric cells with different electrolytes at different current densities.

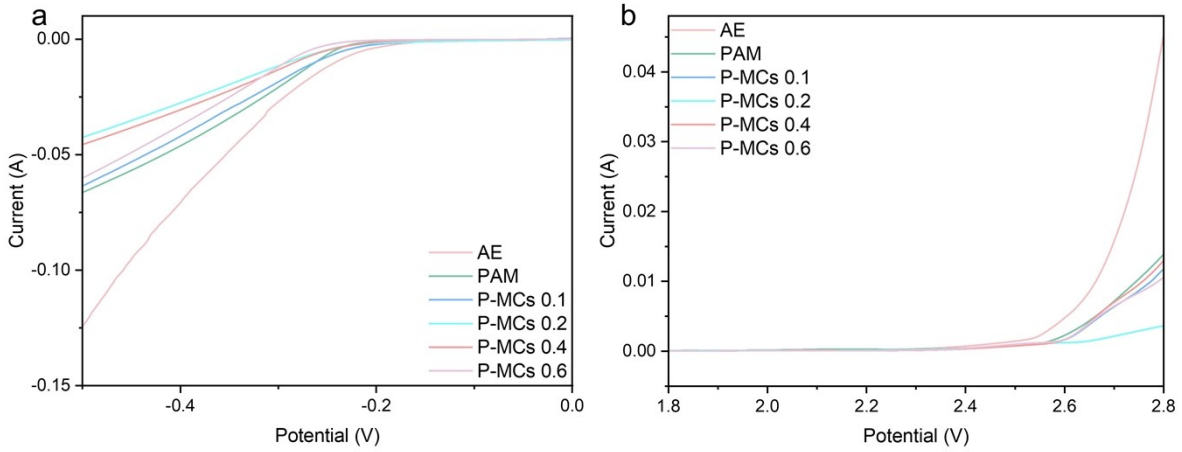

Fig. S31 (a) HER and (b) OER curves of different electrolytes.

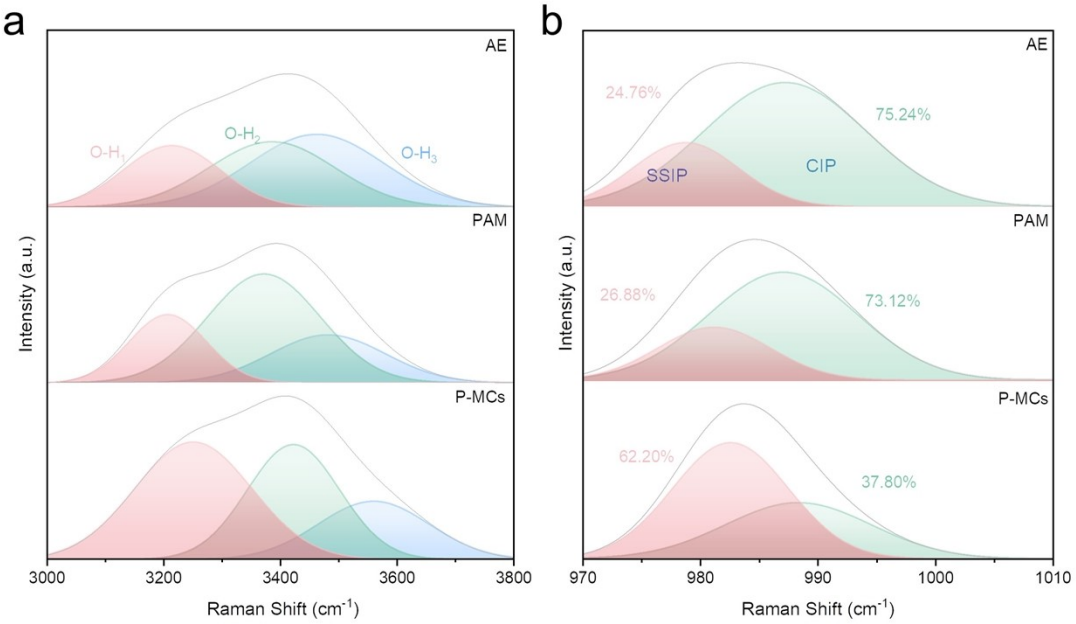

Fig. S32 Raman spectra of (a) *v*-OH^- and (b) *v*-SO_4^{2-} in different electrolytes.

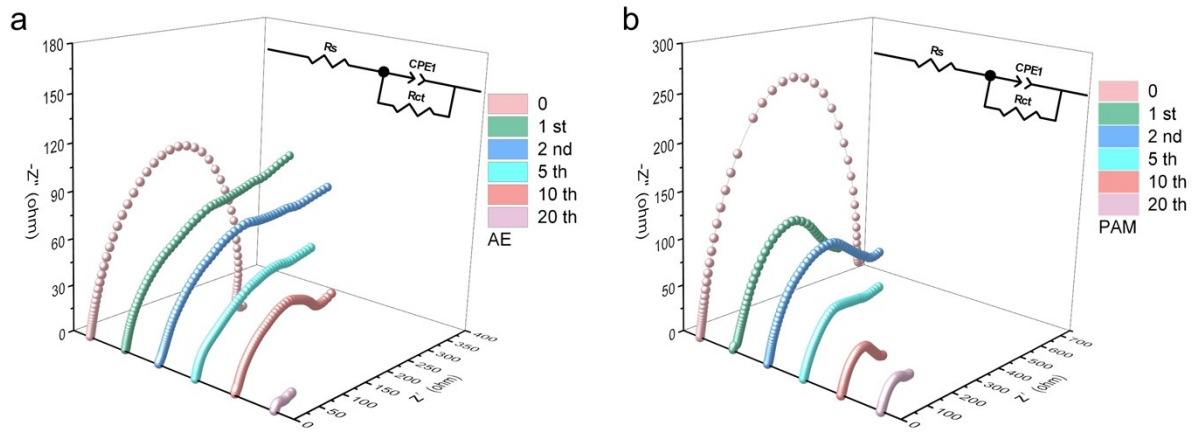

Fig. S33 EIS curves of Zn//Zn symmetric cells with (a) AE and (b) PAM hydrogel electrolyte at different cycles.

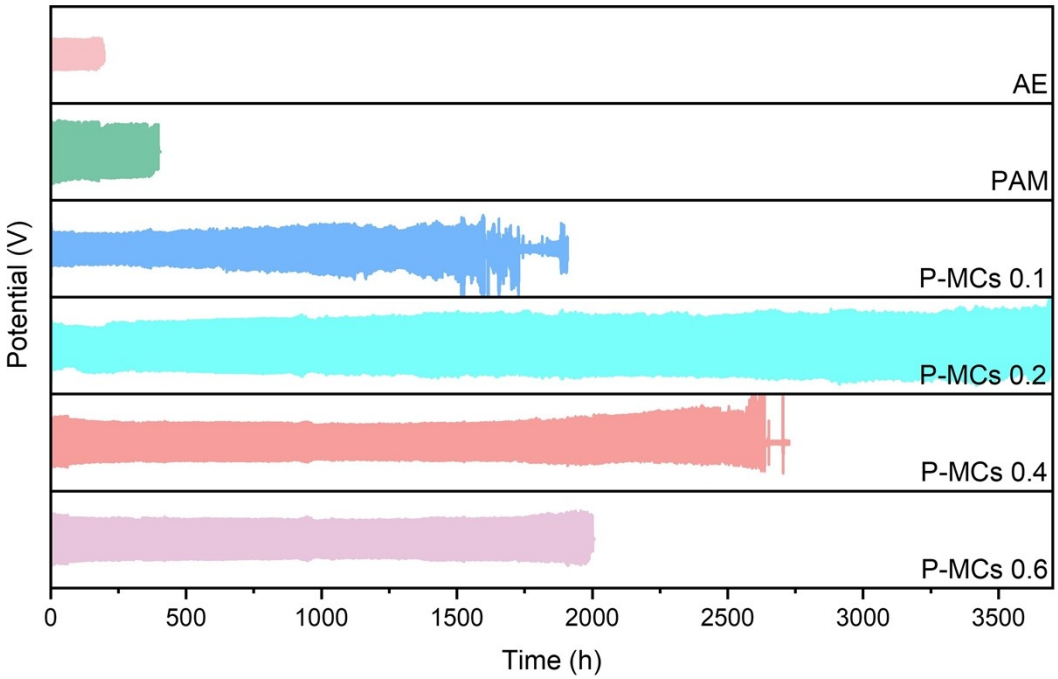

Fig. S34 Cycling performance of Zn//Zn symmetric cells at 1 mA cm^{-2}/1 mAh cm^{-2} of different electrolytes.

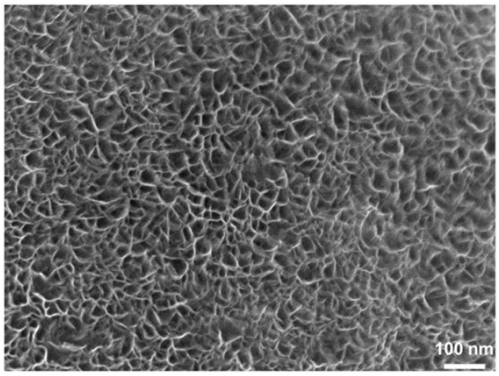

Fig. S35 SEM image of the prepared MnO_2 cathode using the electro-deposition.

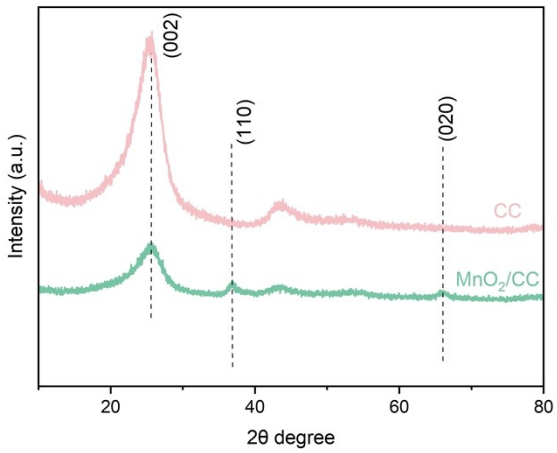

Fig. S36 The XRD pattern of MnO_2 cathode obtained by electrochemical deposition method on carbon cloth.

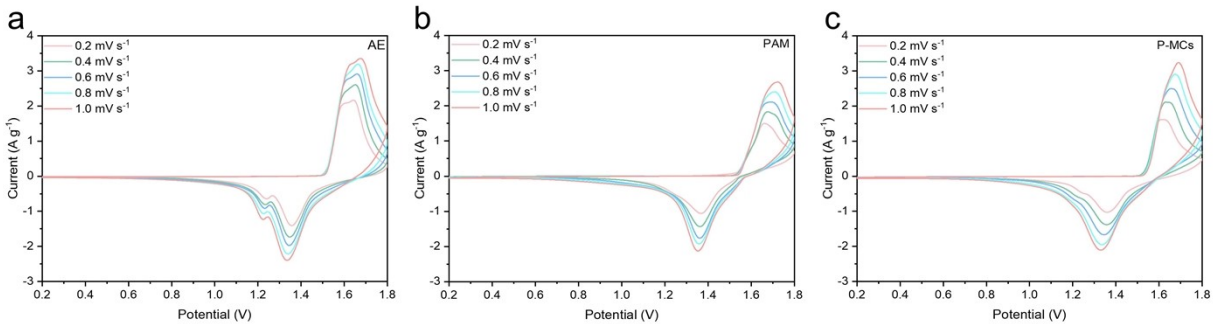

Fig. S37 CV curves of the Zn//MnO_2 full cells with (a) AE, (b) PAM hydrogel electrolyte and (c) P-MCs hydrogel electrolyte from 0.2 to 1.0 mV s^{-1}.

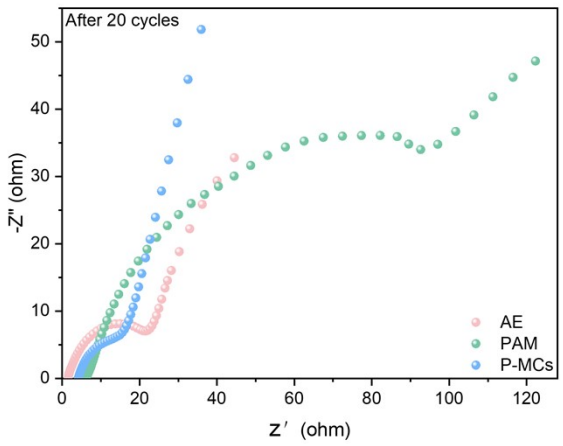

Fig. S38 EIS curves of Zn//MnO_2 cells with different electrolytes after 20 cycles at 1 A g^{-1}.

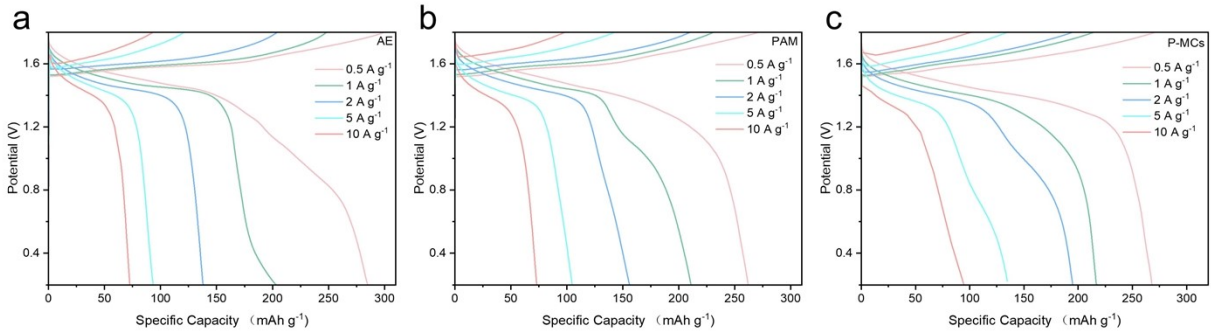

Fig. S39 The discharge/charge curves for Zn//MnO_2 full cells with (a) AE, (b) PAM hydrogel electrolyte and (c) P-MCs hydrogel electrolyte at different current densities.

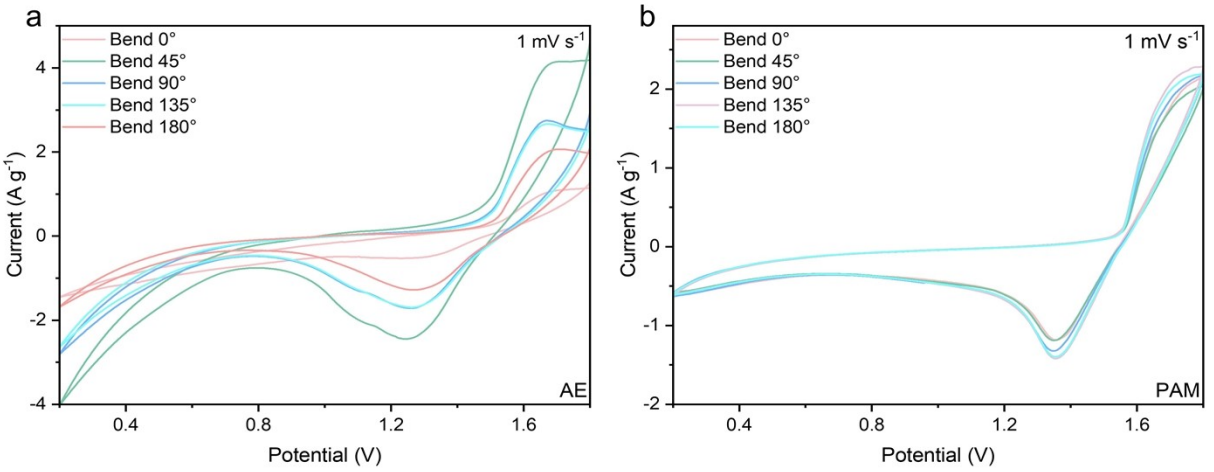

Fig. S40 CV curves of flexible Zn//MnO_2 pouch cells with (a) AE and (b) PAM hydrogel electrolyte at different bending angles.

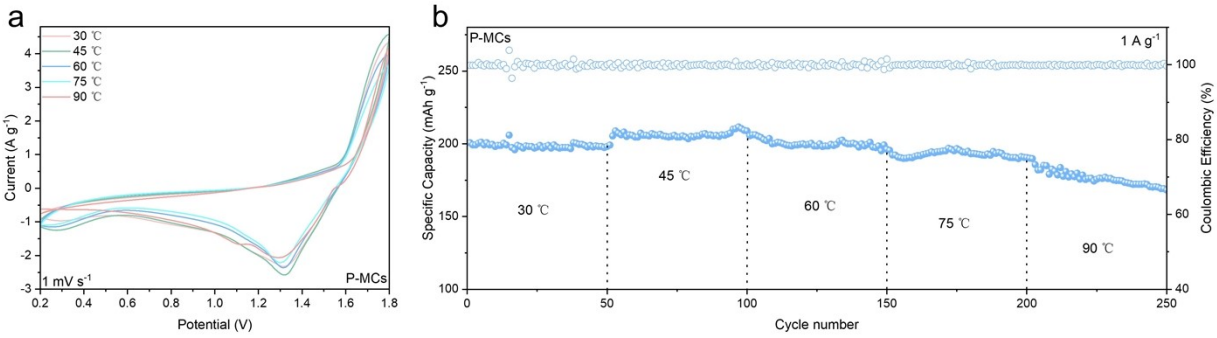

Fig. S41 (a) CV curves and (b) cyclability of flexible Zn//MnO_2 pouch cell under different temperatures at 1 A g^{-1}.

Fig. S42 (a) CV curves and (b) cyclability of flexible Zn//MnO_2 pouch cell under different humidity at 1 A g^{-1}.

Table S1. Performance comparison between different electrolytes-based Zn//Cu cells.

Material	Current density (mA cm^{-2})	Areal capacity (mAh cm^{-2})	Cycle number	Coulombic efficiency (%)	Ref.
6P-PAM	1	1	500	98.6	19
PZIB	1	1	400	99.6	20
PVA-Agar-DMSO	1	1	250	99.02	21
CWK	1	1	600	98	22
CMC/TA	1	1	500	98.31	23
GarraChi	5	1	600	99	24
LAG	4	1	160	99.8	12
PDC-20	1	1	250	99.1	25
PAMPSZn	1	1	250	98.9	8
MGA	10	1	600	99.67	26
$Zn_2(bim)_4$	0.5	0.5	100	98.04	27
PACXHE	4	1	500	97.7	28
$G(DC)_2$	1	1	80	99.6	29
PSCA	2	0.5	100	98.4	30
AG-PAM/Zn	1	1	300	99.48	31
P-MCs	1	1	760	98.2	This work
	5	1	780	98.2	
	10	1	800	98.6	
	20	1	720	98.4	

Table S2. Comparison of other reports and our work in capacity and cycle performance.

Materials	Electrolyte	Capacity (mAh g^{-1})	Cycle performance	Ref.
V_2O_5 nanospheres	2 M $ZnSO_4$	188.7	140 mAh g^{-1} after 1000 cycles at 10 A g^{-1}	32
MnO_2@C	peptide gel electrolyte	250	169.8 mAh g^{-1} after 150 cycles at 0.5 A g^{-1}	5
α-MnO_2/carbon black powder/polyvinylidene	ILG-Zn/MnO_2	180	95.7% (172 mAh g^{-1}) after 600 cycles at 2 C	33
MnO_2/CNT	PZIB gel	210	150 mAh g^{-1} after 1000 cycles at 5C	34
PANI@ SWCNT	$Zn(BF_4)_2$-PAM	106	94% (99.7 mAh g^{-1}) after 1000 cycles at 1A g^{-1}	35
NVO	1 M $ZnSO_4$ and 1 M Na_2SO_4	184.1	98.2% (180.8 mAh g^{-1}) after 500 cycles at 1A g^{-1}	22
SNVP 5	HGE	95	101 mAh g^{-1} after 400 cycles at 1 C	36
PANI	ZSO + LiTFSI	268	122 mAh g^{-1} after 200 cycles at 0.5 C	16
ZnVO	in-situ Gel	410	60.7% (248.87 mAh g^{-1}) after 500 cycles at 1A g^{-1}	37
NVO	MMT-PAM	287.6	89% (256 mAh g^{-1}) after 300 cycles at 0.5 A g^{-1}	38
ZVO	ZGPE-5	378	85% (321.3 mAh g^{-1}) after 600 cycles at 0.5 A g^{-1}	39
α-MnO_2	PAG@GF	350	154.9 mAh g^{-1} after 1000 cycles at 1 A g^{-1}	11
MnO_2	Zn@$Zn_2(bim)_4$	139.5	48% (66.96 mAh g^{-1}) after 600 cycles at 0.5 A g^{-1}	27
MnO_2@CC	P-MCs	199.7	83.14% (166 mAh g^{-1}) after 1000 cycles at 1 A g^{-1}	This work

Reference

1. J. Xu, W. Lv, W. Yang, Y. Jin, Q. Jin, B. Sun, Z. Zhang, T. Wang, L. Zheng, X. Shi, B. Sun and G. Wang, *ACS Nano*, 2022, **16**, 11392–11404.
2. M. C. Schulze and N. R. Neale, *ACS Energy Lett.*, 2021, **6**, 1082-1086.
3. S. Ilic, M. J. Counihan, S. N. Lavan, Y. Yang, Y. Jiang, D. Dhakal, J. Mars, E. N. Antonio, L. Kitsu Iglesias, T. T. Fister, Y. Zhang, E. J. Maginn, M. F. Toney, R. F. Klie, J. G. Connell and S. Tepavcevic, *ACS Energy Lett.*, 2023, **9**, 201-208.
4. S. T. Oyakhire, W. Zhang, Z. Yu, S. E. Holmes, P. Sayavong, S. C. Kim, D. T. Boyle, M. S. Kim, Z. Zhang, Y. Cui and S. F. Bent, *ACS Energy Lett.*, 2023, **8**, 869-877.
5. Y. Wang, X. Liu, R. Ge, M. Moretti, J. Yin, Z. Zhao, A. U. Valle-Pérez, H. Liu, Z. Tian, T. Guo, Y. Zhu, C. A. E. Hauser and H. N. Alshareef, *ACS Nano*, 2023, **18**, 164-167.
6. J. Geng, H. Zhao, K. Zhang, J. Lai, Q. Lv, Q. Zhang, L. Wang and C. Li, *Chem. Eng. J.*, 2024, **496**, 153816.
7. X. Wang, B. Wang and J. Cheng, *Adv. Funct. Mater.*, 2023, **33**, 2304470.
8. J. Cong, X. Shen, Z. Wen, X. Wang, L. Peng, J. Zeng and J. Zhao, *Energy Storage Mater.*, 2020, **35**, 586-594.
9. K. Leng, G. Li, J. Guo, X. Zhang, A. Wang, X. Liu and J. Luo, *Adv. Funct. Mater.*, 2020, **30**, 2001317.
10. Y.-T. Xu, S.-J. Dai, M.-J. Gong, J.-Z. Zhang, H. Xu, A. Li, S.-I. Sasaki, X.-X. Zeng, X.-W. Wu and X.-F. Wang, *Small*, 2023, **20**, 2304463.
11. Z. Xu, Z. Shi, Z. Chang, F. Feng, Z. Liu, D. Chu, J. Ren, Z.-F. Ma, S. Chen and T. Liu, *J. Energy Chem*., 2024, **95**, 29-38.
12. Z. Shi, J. Guo, Z. Liu, Z. Xu, J. Yu, J. Ren, S. Chen and T. Liu, *Adv. Funct. Mater.*, 2024, DOI: 10.1002/adfm.202406568.
13. C. Tian, J. Wang, R. Sun, T. Ali, H. Wang, B.-B. Xie, Y. Zhong and Y. Hu, *Angew. Chem. Int. Ed.*, 2023, **62**, e202310970.

14. Z. Zhang, R. Zhang, Y. Gao, Y. Gao, F. Jia and G. Gao, *Chem. Eng. J.*, 2024, **484**, 149759.

15. W. Hu, Y. Zhang, J. Ju, Y. Wang, Z. Zhang and W. Kang, *Small*, 2023, **20**, 2305140.

16. J. Wu, M. Li, X. Ding, Z. Chen, J. Luo, Q. Zhang, Y. Qiu, Q. Wang, W. Liu and C. Yang, *Small*, 2024, DOI: 10.1002/smll.202400390.

17. L. Yao, C. Hou, M. Liu, H. Chen, Q. Zhao, Y. Zhao, Y. Wang, L. Liu, Z. W. Yin, J. Qiu, S. Li, R. Qin and F. Pan, *Adv. Funct. Mater.*, 2022, **32**, 2209301.

18. J. Feng, D. Ma, K. Ouyang, M. Yang, Y. Wang, J. Qiu, T. Chen, J. Zhao, B. Yong, Y. Xie, H. Mi, L. Sun, C. He and P. Zhang, *Adv. Funct. Mater.*, 2022, **32**, 2207909.

19. H. Wang, W. Wei, X. Liu, S. Xu, Y. Dong and R. He, *Energy Storage Mater.*, 2023, **55**, 597-605.

20. Y. Hao, D. Feng, L. Hou, T. Li, Y. Jiao and P. Wu, *Adv. Sci.*, 2022, **2**, 2104832.

21. M. Li, C. Xi, X. Wang, L. Li, Y. Xiao, Y. Chao, X. Zheng, Z. Liu, Y. Yu and C. Yang, *Small*, 2023, **19**, 2301569.

22. Y. Shao, J. Zhao, W. Hu, Z. Xia, J. Luo, Y. Zhou, L. Zhang, X. Yang, N. Ma, D. Yang, Q. Shi, J. Sun, L. Zhang, J. Hui and Y. Shao, *Small*, 2022, **18**, 2107163.

23. X. Li, Y. Li, R. Wang, D. Wang and F. Ran, *Chem. Eng. J.*, 2024, **496**, 153865.

24. F. Wang, J. Zhang, H. Lu, H. Zhu, Z. Chen, L. Wang, J. Yu, C. You, W. Li, J. Song, Z. Weng, C. Yang and Q.-H. Yang, *Nat. Commun.*, 2023, **14**, 4211.

25. S. Huang, S. He, Y. Li, S. Wang and X. Hou, *Chem. Eng. J.*, 2023, **464**, 142607.

26. J. Zhou, M. Xie, F. Wu, Y. Mei, Y. Hao, L. Li and R. Chen, *Adv. Mater.*, 2021, **34**, 2106897.

27. J. Sun, Q. Jian, B. Liu, P. Lin and T. Zhao, *Energy Environ. Mater.*, 2024, **0**, e12769.

28. C. Jin, C. Yang, H. Mi, C. Ji, F. Guo, C. Liu, Z. Liu and N. Yang, *J. Energy Chem.*, 2023, **86**, 373-381.

29. W. Cai, X. Zhang, G. Li and L. Chen, *Chem. Eng. J.*, 2024, **484**, 149390.

30. G. Guo, C. Ji, H. Mi, C. Yang, M. Li, C. Sun and L. Sun, *Adv. Funct. Mater.*, 2023, **34**, 2308405.

31. M. Zhang, J.-H. Li, Y. Tang, D.-W. Wang, H. Hu, M. Liu, B. Xiao and P.-F. Wang, *Energy Storage Mater.*, 2023, **65**, 103113.

32. F. Liu, Z. Chen, G. Fang, Z. Wang, Y. Cai, B. Tang, J. Zhou and S. Liang, *Nano-Micro Lett.*, 2019, **11**, 25.

33. D. Lee, H. I. Kim, W. Y. Kim, S. K. Cho, K. Baek, K. Jeong, D. B. Ahn, S. Park, S. J. Kang and S. Y. Lee, *Adv. Funct. Mater.*, 2021, **31**, 2103850.

34. Y. Hao, D. Feng, L. Hou, T. Li, Y. Jiao and P. Wu, *Adv. Sci.*, 2022, **9**, 2104832.

35. Y. Shi, R. Wang, S. Bi, M. Yang, L. Liu and Z. Niu, *Adv. Funct. Mater.*, 2023, **33**, 2214546.

36. X. Lin, G. Zhou, J. Liu, M. J. Robson, J. Yu, Y. Wang, Z. Zhang, S. C. T. Kwok and F. Ciucci, *Adv. Funct. Mater.*, 2021, **31**, 2105717.

37. Y. Wang, L. Yang, P. Xu, L. Liu, S. Li, Y. Zhao, R. Qin and F. Pan, *Small*, 2023, **20**, 2307446.

38. S. Ji, J. Qin, S. Yang, P. Shen, Y. Hu, K. Yang, H. Luo and J. Xu, *Energy Storage Mater.*, 2022, **55**, 236-243.

39. S. Lee, I. K. Han, N. G. Jeon, Y. Lee, H. B. Son, D.-Y. Han, S. Nam, T. Chung, M.-J. Kwak, Y. S. Kim and S. Park, *Adv. Sci.*, 2023, **10**, 2304915.